

Nitrogen isoelectronic trap in GaAs_{1-x}P_x: II. Model calculation of the electronic states N_Γ and N_X at low temperature

William Y. Hsu* and John D. Dow*

Department of Physics and Materials Research Laboratory, University of Illinois at Urbana-Champaign, Urbana, Illinois 61801

D. J. Wolford† and B. G. Streetman†

Department of Electrical Engineering and Coordinated Science Laboratory, University of Illinois at Urbana-Champaign, Urbana, Illinois 61801

(Received 3 March 1977)

A semiphenomenological theory of the isolated N isoelectronic trap in GaAs_{1-x}P_x is presented, based on an extended (multisite), one-band Koster-Slater model of the electron-impurity interaction, including the effects of both the central-cell atomic pseudopotential difference and the spatially extended lattice distortion surrounding the substitutional nitrogen impurity. The alloy host is treated in a virtual-crystal approximation. The parameters of the model are determined by fitting low-temperature photoluminescence data from ion-implanted materials of two compositions selected near $x \approx 0.35$. The model yields both a spatially localized N_X (or A) state which evolves continuously with decreasing x from the A line of GaP, and a spatially-diffuse state N_Γ which is present in near-direct and direct-band-gap alloys ($0.3 \lesssim x \lesssim 0.5$). The theory quantitatively describes the energies of these luminescence lines as a function of alloy composition x . In addition, good agreement with the data is found for the following calculated quantities: (i) the composition dependences of the N_Γ and N_X luminescence intensities, (ii) the pressure dependences of the N_Γ and N_X intensities, (iii) the composition dependence of the N_X lifetime, and (iv) the binding energy of NN_1 pairs in GaP. The model leads to a tentative interpretation of N_Γ luminescence as originating, at least in part, from excitonic molecules.

I. INTRODUCTION

Six main facts which a theory of low-temperature luminescence from excitons bound to the isolated nitrogen isoelectronic trap in GaAs_{1-x}P_x alloys must explain are: (i) that the A (or N_X) line of GaP is observed for $x > 0.24$ in the ternary alloy¹⁻⁷ (where it is called the N_X line) with an energy which continuously evolves as a function of x from the GaP A -line energy,¹ $E(N_X) \approx (1.682 + 0.538x + 0.094x^2)$ eV; (ii) that an additional line N_Γ appears for^{4,5} $0.28 \lesssim x \lesssim 0.5$, with energy¹ $E(N_\Gamma) \approx (1.334 + 2.182x - 1.372x^2)$; (iii) that the isolated-impurity N_X or A state in GaP is believed to be a shallow-impurity state lying only 11 meV below the free-exciton edge,^{8,9} even though nearest-neighbor nitrogen pairs give rise to a very deep NN_1 impurity level ≈ 132 meV lower⁸; (iv) that the ratio of $N_\Gamma:N_X$ luminescence intensities, as a function of composition x , has a maximum near $x \approx 0.37$; (v) that the intensities I of the N_Γ and N_X lines decrease exponentially with the application of pressure,⁵ $I \propto e^{-\alpha P}$ (the coefficients α have been measured for selected compositions); and (vi) that the lifetime of the N_X luminescence decreases exponentially with decreasing phosphorus content.¹⁰ We present here a semiphenomenological theory which accounts for these facts; the parameters of our theory are determined empirically from the GaAs_{1-x}P_x:N luminescence spectra at two alloy compositions x near $x \approx 0.35$.

A. Data

The experimental data¹ are summarized in the alloy composition diagram (Fig. 1), which depicts the positions of discernible photoluminescence peaks at each alloy composition. In analyzing the photoluminescence data, it is customary to assume that the photogenerated electrons and holes relax into equilibrium with the lattice in $\sim 10^{-13}$ sec; the relaxed electron and hole distributions exhibit quasi-Fermi-energies determined by the exciting-light intensity and recombine in $\geq 10^{-9}$ sec.^{10,11} Since the data are taken at liquid-helium temperature, thermal excitation and broadening is negligible, and the electron and hole quasi-Fermi-functions are essentially step functions on the scale of Fig. 1. In spite of various radiative and nonradiative transitions, one may assume that the electrons reach a quasiequilibrium and are appropriately describable by the usual quasi-Fermi-statistics. In interpreting the data, it is convenient to ignore the electron-hole interaction since the exciton binding energy (4.2 meV in¹² GaAs and between^{13,14} 10 and⁹ 17 meV in GaP) is negligible on the scale of interest. Thus we shall discuss the physics of the alloys in terms of the virtual-crystal one-electron band structure,¹⁵ which varies continuously from the infrared¹⁶ (1.5194 eV at 2 °K) direct-band-gap structure of GaAs to the green⁹ (assumed 2.345 eV at 0 °K) indirect-gap structure of GaP (Fig. 2).

butable to variation of relative electronegativity and valence charge transfer in the alloys.)

Altarelli's extension²¹ of the Scifres *et al.* model²⁰ to treat the case of an N_x level resonant with the Γ density-of-states continuum provides an apt description of such resonances; however, the Altarelli model dealt with the previous interpretation of nitrogen luminescence data.¹⁹ It is now clear that the resonance effect, if present, must occur¹ near $x \approx 0.24$ rather than $x \approx 0.40$ as originally assumed.¹⁹

Recently Aspnes *et al.*²² have reported measurements indicating that the L -band minima in GaAs and in the direct-gap compositions of $\text{GaAs}_{1-x}\text{P}_x$ occur at lower energies than previously believed.^{20,26} Based on these measurements and a simplified two-minima approximation, these authors have proposed that the L minima play a dominant role in determining the binding of the N_x level in $\text{GaAs}_{1-x}\text{P}_x$. Absent from the Aspnes treatment are couplings among different parts of the Brillouin zone. In Appendix A we solve the Aspnes model exactly without resorting to the two-minima approximation; we find that the exact and approximate solutions disagree with one another and with the data.

In recent work, Kleiman *et al.*²³ have presented an interpretation of the nitrogen luminescence which differs from that originally presented by Wolford *et al.*^{3,4} and used by Nelson *et al.*⁵ The Kleiman *et al.* theory assumes that both N_Γ and N_x originate from the long-ranged strain tail of the potential, and that an additional state N is bound by the short-ranged isoelectronic potential. Hence the theory seems to imply that N_x and N_Γ do not depend on the details of the central-cell short-ranged binding.²⁷ Since this binding, attributed to the nitrogen-anion electronegativity difference, is dominant for the A (or N_x) line in GaP,⁸ it should also play an important role for N_x in $\text{GaAs}_{1-x}\text{P}_x$. In the theory to be presented here, the short-ranged potential which gives rise to the GaP A line is deepened continuously in the ternary, where it is referred to as N_x .

The data of Fig. 1 do not support the prediction²³ that there should be a line N for $x > 0.5$. (See Appendix B for a summary of the model of Kleiman *et al.*) The spectral data from our nitrogen-ion-implantation studies result from liquid-helium-temperature photoluminescence measurements on bulk-geometry samples of light donor doping ($\sim 10^{15}$ – 10^{17} cm^{-3}) and negligible acceptor compensation.^{3,4,7} Data from the indicated alloy compositions of Fig. 1 are based on measurements over the wide range of peak nitrogen concentrations $10^{16} \leq N_N \leq 10^{20}$ cm^{-3} achievable by implantation. Because of these experimental conditions, the

data of Fig. 1 are free of (i) thermal line broadening and carrier detrapping from shallow levels which are common at higher temperatures, (ii) spectral variations caused by cavity modes in thin $\text{GaAs}_{1-x}\text{P}_x$ samples, and (iii) the undesirable effects of high donor or acceptor concentrations, which can shift peak energies, and broaden and distort both band-edge and nitrogen related luminescence.^{1,7} We have observed such distortions and peak shifts in the presence of high donor and/or acceptor concentrations (common in electroluminescent devices). As a result, we expect the data of Fig. 1 to faithfully reveal the dominant features of nitrogen luminescence states.

II. GENERAL FEATURES OF THE SPECTRA

An examination of the data (Fig. 1) reveals the assumed Γ_1 and X_1 band-edge dependences, the prominent nitrogen-trap emission line N_x , a distinct line¹ N_Γ also related to the nitrogen trap, and phonon sidebands of N_x .²⁸ Spectral lines associated with excitons bound to donors are not displayed in Fig. 1, but are discussed elsewhere.⁴

Here we are concerned with the lines N_Γ and N_x , both of which we associate with isolated nitrogen centers. Evidence supporting this identification is based on extensive studies^{1-4,6,7} of the dependence of the luminescence spectra on nitrogen concentration, implant depth profile,²⁹ alloy composition, implanted species other than nitrogen, and annealing results.^{7,29}

The facts that N_Γ appears to be "attached" to the Γ_1 band edge, following it as x varies, and that N_Γ appears without prominent phonon sidebands, are reminiscent of an effective-mass-like shallow-impurity state,³⁰ and cause us to examine the possibility that N_Γ may be attributed to a spatially more extended nitrogen-trap state than N_x .

The possibility that the N_Γ and N_x lines are associated with two different types of nitrogen centers in different environments (e.g., an isolated nitrogen and a nitrogen-vacancy pair) appears to be inconsistent with the observed dependence of luminescence data on exciting light intensity—and therefore electron and hole quasi-Fermi-energies (see Table I). If two different nitrogen impurity centers were responsible for N_Γ and N_x luminescence, then N_Γ would be the quasi-ground-state of one center (see Fig. 3). Consequently, at sufficiently low nitrogen concentrations such that inter-nitrogen distances are large, electron transfer at low temperatures from N_Γ to N_x would be forbidden, because the N_Γ - N_x wave-function overlap would be negligible. As a result, N_Γ and N_x would be unable to come into thermal equilibrium with each other. Therefore, with low-level photoexci-

TABLE I. Observed relative emission intensities I (in arbitrary units) as functions of the power P of the exciting light beam (in mW) of the lines N_Γ and N_X . The data were taken at 5 K in $\text{GaAs}_{0.665}\text{P}_{0.335}$ containing $\sim 5 \times 10^{17} \text{ cm}^{-3}$ nitrogen. The sample was annealed for 30 min at 950 C. Saturation sets in between 40 and 50 mW; below saturation the data are well described by $I \propto P^\beta$ with $\beta(N_\Gamma) \approx 1.41$ and $\beta(N_X) \approx 0.83$. The estimated uncertainty of the emission intensities is $\pm 5\%$.

P (mW)	$I(N_\Gamma)$	$I(N_X)$
5	0.089	0.313
10	0.218	0.56
20	0.624	1.00
40	1.57	1.73
50	2.04	2.00
60	2.42	2.24

tation above the band gap, one should expect to observe N_Γ luminescence as well as N_X luminescence, because the local ground state N_Γ could not decay to N_X . Instead, one observes only N_X emission for this case, which is characteristic of efficient $N_\Gamma \rightarrow N_X$ transfer, as one would expect if N_Γ and N_X were both states of a single center and therefore strongly coupled. (See Figs. 3 and 4 and Table I.) Calculations supporting this qualitative analysis are given in Appendix C.

Having settled on a single-center model of the nitrogen trap, with two bound energy levels per trap, N_Γ and N_X , and with N_Γ appearing in direct-band-gap alloys and unstable to decay into N_X , we

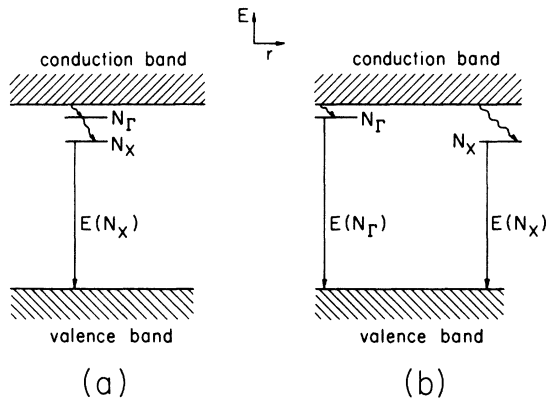


FIG. 3. Sketch of energy levels vs position in (a) one-site model, and (b) two-site model. In the one-site model $N_\Gamma \rightarrow N_X$ nonradiative decay (wavy line) is efficient and at low excitation levels one observes only N_X emission. In the two-site model, N_Γ and N_X are associated with two different isolated sites. At sufficiently low temperature and moderate doping, such that the sites are sufficiently distant, $N_\Gamma \rightarrow N_X$ transfer is negligible. Then, at low excitation levels one should observe both N_Γ and N_X , whereas only N_X is observed (Fig. 4).

have adopted a model which either (i) allows more than one exciton to bind to a given nitrogen impurity, or (ii) permits only one of the two states N_Γ and N_X to be occupied at a given instant. We currently favor the former interpretation: an excitonic molecule model.³¹ Exciton-exciton interaction energies in these alloys are not well known, but in GaP they are³² ~ 2 meV—negligible on the scale of alloy broadening. In the highly polarizable As-rich direct-composition alloys, one expects the electronic contribution to the exciton-exciton interaction to be even weaker than in GaP; changes in the lattice-polarization contributions to the interaction seem unlikely to be of the order (100 meV near $x \approx 0.4$) required to prevent binding of two excitons to a single site. A check on the excitonic molecule interpretation is afforded by studying the dependence of the N_Γ and N_X luminescence intensities on exciting light intensity: the observed (Fig. 4) N_Γ emission is nearly the square of the N_X emission, a characteristic of emission from a molecule³³⁻³⁵ consisting of an N_Γ exciton interacting with an exciton in state N_X .

Hence, we propose an interpretation of the spectra as follows: the lines N_Γ and N_X are associated with excitons bound to isolated nitrogen impurities. The $N_\Gamma \rightarrow N_X$ decay rate is sufficiently fast (when N_X is unoccupied) that light emission from a single N_Γ exciton bound to a nitrogen impurity becomes improbable; however, saturation excitation fills the N_X state,⁷ prevents $N_\Gamma \rightarrow N_X$ transfer, and leads to observable N_Γ luminescence (assumed to be perturbed only slightly by the N_X exciton bound to the same nitrogen site). Because the exciton-exciton

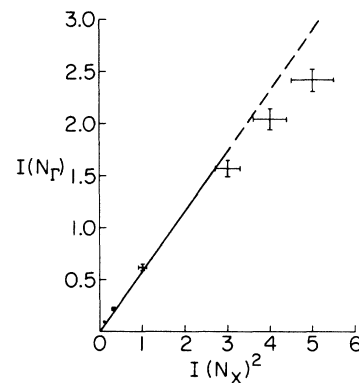


FIG. 4. Intensity of N_Γ luminescence $I(N_\Gamma)$ against the square of N_X luminescence intensity $I(N_X)^2$, for $\text{GaAs}_{0.665}\text{P}_{0.335}$ at 5 K with $\sim 5 \times 10^{17} \text{ cm}^{-3}$ nitrogen. The error bars on the low-intensity data are comparable with the sizes of the plotted rectangles. Saturation sets in where the line becomes dashed. Note that the N_Γ emission becomes negligible in comparison with that of N_X at low excitation levels, and that the N_Γ intensity is almost proportional to the square of the N_X intensity.

interactions are expected to be negligible on the scale of interest, we shall perform all calculations for single excitons associated with the N_Γ or N_X bound states at isolated nitrogen. When comparing computed luminescence intensities with data, we shall consider data taken at saturation excitation.

III. MODEL

A. Physical picture

The nitrogen impurity substitutes for P or As and gives rise to an electron-attractive potential which, in the present model, has two bound states N_Γ and N_X . The usual treatment of the isoelectronic trap treats the host alloy in the virtual-crystal approximation¹⁵ and models the nitrogen potential by a zero-ranged (δ function), composition-independent Koster-Slater potential which attracts a conduction-band electron.²⁰ This potential binds at most one state,²⁵ regardless of the nature of the conduction-band structure and density of states; it also fails to explain the alloy composition dependence of the binding energy of the N_X state relative to the band minima at X . Therefore the zero-ranged, composition-independent Koster-Slater model must be replaced by a spatially extended, composition-dependent potential if two states N_Γ and N_X are to be bound and their energies properly described.

Since the nitrogen is isovalent to and substitutional for P or As, the extended potential range must be attributed to lattice relaxation around the smaller N atom,³⁶ and to the electronic charge redistribution caused by this relaxation. Evidence supporting the role of lattice distortion includes: (i) both the binding energy of N_X relative to the X_1 conduction-band edge and the size mismatch between nitrogen and the virtual-crystal anion ($\text{As}_{1-x}\text{P}_x$) increase monotonically with increasing As concentration; (ii) in the two binary limits, GaAs and GaP, relevant physical quantities, such as the reduced shear elastic constants and the Debye temperature (compiled in Ref. 1), indicate that GaAs is softer and more responsive to stress than is¹ GaP; and (iii) in phosphorus-rich material, the N_X binding energy, the associated Stokes shift, and the exciton-phonon coupling strength all increase dramatically with the replacement of P by As.¹

In addition to the composition-dependent effects of lattice distortion discussed above, the variation with x of the potential is associated with the fact that the screened difference between the ionic pseudopotentials for nitrogen and the host virtual-crystal anion changes with composition. Therefore, lattice deformations and redistribution of electronic charge both should lead to a stronger,

more spatially extended nitrogen potential as the As mole fraction is increased.

If, as seems to be the case, the lattice distortion around the N impurity plays a significant role in binding an electron, then the nitrogen potential is almost certainly not spherically symmetric; the absence of rotational invariance in the potential is further complicated by the anisotropic electron-band structure.^{37,38} *A priori* computation of the potential, wave functions, and energy levels of the nitrogen trap is therefore likely to be difficult, and presently available theoretical techniques appear incapable of producing reliable predictions of energy levels with the needed accuracy³⁸ (~ 5 meV). To circumvent this difficulty we turn to a phenomenological model, replacing the nitrogen potential by an *empirical effective potential* with parameters fixed by experimental data from a limited region of alloy compositions (near $x \approx 0.35$). Thus, to some extent, the effective-potential method embraces in its empirical parameters those details of the nitrogen trap which are incompletely understood at present. Of course, such a method is useful only if its predictions are independent of the detailed form of the effective potential; to check this, we have employed various forms, all of which have two essential features: a strong attractive central cell part and a moderately ranged attractive tail.

Using the effective-mass approximation,^{30,39,40} we have shown that a nitrogen potential of the form $V(r) = -V_0 \text{sech}^2(r/a)$ produces good agreement with the direct-composition ($x < 0.45$) GaAs_{1-x}P_x photoluminescence data.⁴ The same conclusion holds for a square-well potential with similar parameters V_0 and a .⁴¹ Hence, the expectation that almost any effective potential with a nonzero range can reproduce the data for a wide range of GaAs_{1-x}P_x alloys appears to be justified, provided the effective potential's parameters are determined empirically.

The effective-mass approximation^{30,39,40}—although of limited quantitative validity for deep, localized traps such as nitrogen—provides a simple *qualitative* physical picture of the states N_X and N_Γ . If the conduction-band structure of GaAs_{1-x}P_x is partitioned into regions near the X minima and near the Γ minimum, the X minima have heavy density-of-states effective masses⁴² ($m_X^*/m = 0.35 + 0.015x$), whereas the Γ mass is light⁴³ ($m_\Gamma^*/m = 0.063 + 0.052x$). Therefore, an electron whose k -space wave function is localized near zone center will, by virtue of its small mass and large quantum kinetic energy, be incapable of residing deep in the nitrogen potential. Instead, it will occupy a spatially extended, shallow state (with long-wavelength $k \approx 0$ wave-function compo-

nents) which is only weakly bound. In contrast, an electron near X will have a heavy mass and fall deep into the potential well, occupying a deeply bound, localized state. Hence the nitrogen trap, by virtue of the two conduction-band effective masses, can bind two states: one primarily associated with the Γ_1 band edge (N_Γ), and the other associated with the X_1 minima and a larger portion of the Brillouin zone (N_X).

A caveat about using this simple effective-mass picture is in order: a quantitative theory requires a full treatment of the entire Brillouin zone, including valley-orbit couplings among the different regions near X and Γ of the zone.³⁰ Such a treatment, when applied to short-ranged forces, can significantly modify the picture; for example, a one-site (δ function) Koster-Slater potential will produce several bound states, each associated with a different conduction-band minimum in the zeroth-order effective-mass approximation, but only one in the exact calculation which accounts for the full Brillouin zone.

B. Extended Koster-Slater model

From an operational viewpoint, the most suitable form for the effective potential is one which is simple, leads to tractable computations, and contains all the physical features necessary to reproduce the data and successfully predict the outcome of experiments. One of the difficult technical problems met in treating impurities in multivalley semiconductors occurs when one attempts to couple different regions of the Brillouin zone (valley-orbit coupling) and arises because one naturally solves the Schrödinger equation in such a system by finding solutions to effective-mass equations valid near each of the multiple minima. The valley-orbit coupling problem can be completely circumvented by simultaneously treating the interaction of the impurity with all of the valleys, a treatment which is feasible only if the impurity potential belongs to a very restricted class of potentials.⁴⁴ Therefore, to simplify our computations, we select a potential from this restricted class: an extended Koster-Slater potential⁴⁴ which affects only those electrons contacting the nitrogen impurity cell or one of its 12 nearest-neighbor primitive cells:

$$V = \sum_{i,j=0}^{12} |W(\vec{R}_i)\rangle V_{ij} \langle W(\vec{R}_j)|. \quad (1)$$

Here the summation ranges over only the central cell and the 12 nearest-neighbor cells, and the states $|W(\vec{R}_i)\rangle$ are conduction-band Wannier functions centered at the anion (column V) site \vec{R}_i .

Physically this model contains an attractive central-site interaction which approximates the screened potential difference between a nitrogen impurity and the anion it replaces. The effects of lattice distortion surrounding each nitrogen is lumped into interactions among the nearest-neighbor anion sites; this simulation tends to overestimate the short-ranged parts of the deformation potential at the expense of longer-ranged parts.

The Schrödinger equation for an electron in the state $|\psi\rangle$ bound by this potential to the nitrogen impurity is

$$|\psi\rangle = (E - H_0)^{-1} V |\psi\rangle, \quad (2)$$

where H_0 is the conduction-band Hamiltonian with eigenvalues $E(\vec{k})$ and eigenfunctions $|B(\vec{k})\rangle$

$$H_0 |B(\vec{k})\rangle = E(\vec{k}) |B(\vec{k})\rangle. \quad (3)$$

The Bloch functions $|B(\vec{k})\rangle$ are related to the Wannier functions by

$$|W(\vec{R})\rangle = \frac{(2\pi)^{3/2}}{V_0^{1/2}} \sum_{\vec{k}} |B(\vec{k})\rangle e^{-i\vec{k}\cdot\vec{R}}, \quad (4)$$

where the normalization volume V_0 is the volume of the primitive cell and the sum is restricted to wave vectors in the first Brillouin zone. The energy E , when near an eigenvalue of H_0 , is to be interpreted in the scattering-wave boundary-condition sense: as the limit of vanishingly small ϵ of $E + i\epsilon$.

In a Wannier function basis the extended Koster-Slater model reduces the integral equation (2) to a set of linear algebraic equations:

$$\langle W(\vec{R}_i) | \psi \rangle = \sum_{j=0}^{12} \langle W(\vec{R}_i) | \frac{1}{E - H_0} V | W(\vec{R}_j) \rangle \langle W(\vec{R}_j) | \psi \rangle. \quad (5)$$

Here \vec{R}_i runs over all primitive cells, but only 13 values of \vec{R}_j are required for this model potential. Only 13 of the \vec{R}_i are needed to determine the bound-state energies E (13 being one greater than the number of nearest-neighbor anions); the secular equation is

$$\det[\delta_{i,j} - \langle W(\vec{R}_i) | (E - H_0)^{-1} V | W(\vec{R}_j) \rangle] = 0, \quad (6)$$

where i and j range from zero to 12. Solution of the 13 algebraic equations is facilitated by the assumption that the nitrogen potential transforms according to the point group of the anion site in the zinc-blende structure.⁴⁵ Then $(E - H_0)^{-1} V$ has the tetrahedral symmetry T_d , and the eigenfunctions may be chosen to transform according to the irreducible representations of T_d . Group theory may then be employed to exploit the symmetry and to partially diagonalize the system of equations by determining the linear combinations of Wannier

TABLE II. Character table for the T_d group: the first five rows are for the irreducible representations whereas the last row is for the reducible representation D formed from the 13 conduction-band Wannier functions localized at the impurity cell and its 12 nearest-neighboring cells.

	E	$3C_2^4$	$6S_4$	$6C_4$	$8C_3$
A_1	1	1	1	1	1
A_2	1	1	-1	-1	1
E	2	2	0	0	-1
T_1	3	-1	1	-1	0
T_2	3	-1	-1	1	0
D	13	1	1	3	1

functions which transform according to the appropriate irreducible representations; these new basis functions reduce the secular determinant to block diagonal form. The character table of the group (in the notation of Tinkham⁴⁶) is reproduced in Table II. With respect to an origin at an anion site, the central-cell conduction-band Wannier function $|W(0)\rangle$ is known to be s -like and transforms according to the trivial representation A_1 .⁴⁷ The 13 Wannier functions centered on the central site and its neighbors form a basis for a reducible representation D whose character may be determined by simply counting the number of spheres (A_1 contours) mounted on those sites unmoved by group operations of each class. This character is given in Table II and can be reduced using standard techniques^{46,48}: D decomposes into irreducible representations

$$D \rightarrow 2A_1 + E + T_1 + 2T_2. \quad (7)$$

This will result in the factoring of the secular determinant into a 2×2 A_1 determinant, a 2×2 E determinant, a 3×3 T_1 determinant, and a 6×6 T_2 determinant, thereby reducing the determinant [Eq. (6)] to block form. As pointed out in Appendix D, only the totally symmetric states A_1 are likely to bind electrons; hence, we focus our attention on the 2×2 A_1 determinant with basis functions for the 0th shell (central cell) and the 1st shell (of neighboring cells) transforming according to A_1

$$|0\rangle \equiv |A_1, 0\rangle \equiv |W(0)\rangle, \quad (8a)$$

$$|1\rangle \equiv |A_1, 1\rangle \equiv (12)^{-1/2} \sum_{i=1}^{12} |W(\vec{R}_i)\rangle, \quad (8b)$$

$$\begin{vmatrix} 1 - \langle 0 | (E - H_0)^{-1} V | 0 \rangle & -\langle 0 | (E - H_0)^{-1} V | 1 \rangle \\ -\langle 1 | (E - H_0)^{-1} V | 0 \rangle & 1 - \langle 1 | (E - H_0)^{-1} V | 1 \rangle \end{vmatrix} = 0. \quad (9)$$

The solutions of this determinantal equation are the

eigenenergies $E(N_x)$ and $E(N_r)$. The determinant's elements are evaluated in Appendix E, where it is shown that, in the local approximation, $E(N_x)$ is the solution of

$$\sum_{\vec{k}}^{\text{1BZ}} \frac{1}{E(N_x) - E(\vec{k})} = + \frac{1}{\langle 0 | V | 0 \rangle} \equiv -\frac{1}{J}. \quad (10)$$

The sum is restricted to wave vectors in the first Brillouin zone, and we have introduced Faulkner's⁴⁷ strength parameter J . Similarly $E(N_r)$ is approximately the solution of the equation

$$\sum_{i,r=1}^{12} \sum_{\vec{k}}^{\text{1BZ}} \frac{1}{E(N_r) - E(\vec{k})} e^{i\vec{k} \cdot (\vec{R}_i - \vec{R}_r)} = -\frac{12}{L}, \quad (11)$$

where L is a sum of matrix elements V_{ij} given in Appendix E. The corresponding wave functions are also given in Appendix E.

A noteworthy feature of Eqs. (10) and (11) is that neither depends on the conduction-band Bloch functions, except through the parameters J and L , which are fixed empirically. A knowledge of the conduction-band structure $E(\vec{k})$ is sufficient to evaluate these equations (the details of this evaluation are documented in Appendix F). This particularly simple form is a consequence of the one-band Koster-Slater model, which, from an *a priori* viewpoint, is quite crude. A more realistic model would replace the Koster-Slater potential with apt isoelectronic and strain fields and would employ a many-band formalism,⁴⁹ constructing the nitrogen-site wave function from Bloch waves associated with several host-crystal bands. Nevertheless, for a semiphenomenological theory, the simplicity of the present model outweighs its deficiencies.

C. Determination of the parameters J and L

The electron-nitrogen interaction and the parameters J and L should depend on the composition x of the GaAs_{1-x}P_x alloy because covalent-bond screening and lattice distortion surrounding a nitrogen will vary with x . Here we postulate simple linear dependences of J and L on x , a form suggested by Vegard's law⁵⁰ for the lattice constant:

$$J = J_0 + J_1 x, \quad L = L_0 + L_1 x.$$

The four parameters are determined by fitting the observed energies $E(N_r)$ and $E(N_x)$ near $x \approx 0.35$. The resulting values are $J_0 = -0.6796$ eV, $J_1 = 0.1126$ eV, $L_0 = -0.7959$ eV, $L_1 = 0.5371$ eV. Note that as expected on physical grounds, the central-cell potential J is a weak function of x , whereas L , which simulates the moderate-ranged strain tail, varies considerably from GaAs to GaP. It

should be stressed that the assumed linear dependence of the potential strength on x does not, by itself, produce the observed nearly linear variation of the N_x energy. The redistribution of the conduction-band density of states (with increasing x , the Γ_1 and L_1 minima move to higher energy faster than the X_1 minima) and the reduction in potential strength with increasing x play comparable roles in determining the energy of the nitrogen trap.

IV. RESULTS

A. Energies

1. Isolated nitrogen in $GaAs_{1-x}P_x$

The energies of the lines N_Γ and N_x computed from Eqs. (10) and (11) are given in Fig. 5 and are in excellent agreement with the data. Even though the parameters of the potential are determined empirically from spectra of arsenic-rich alloys with $x \approx 0.35$, the model (i) predicts the energy of the A line in GaP ($x=1$), (ii) reproduces the observed N_Γ and N_x energies for all alloy compositions x , and (iii) explains the absence of nitrogen bound states for $x \leq 0.2$, the presence of two bound states for $0.2 \leq x \leq 0.5$, and the presence of only one for $x > 0.5$. The theory does not treat the observed evolution of N_Γ into $N_{\Gamma-x}$ near $x \approx 0.5$.²⁸

2. Nitrogen pairs in GaP

An independent check of the model is afforded by computing the energy of the NN_1 pair state in GaP. Faulkner, in his original treatment of the A line in GaP,⁴⁷ employed a single-site one-band Koster-Slater model of the nitrogen impurity potential with the strength of the potential determined by the ob-

served binding energy of the A line in GaP. Using two such potentials for nearest-neighbor nitrogen pairs, Faulkner calculated the NN_1 pair binding energy to be ~ 163 meV, compared with the experimental value of ~ 143 meV.⁸ He then modified his nitrogen potential, giving it a nonzero range, and found a binding energy of ~ 195 meV.

Following Faulkner, we have evaluated the NN_1 pair energy in GaP for the nitrogen impurity potential of the present work. The resulting binding energy is ~ 294 meV, sufficiently close to the experimental value to reassure us that the basic model is sound (remember that the parameters J and L of the present model were determined by fitting alloy spectra for $x \approx 0.35$, whereas Faulkner fit GaP data). An encouraging feature of the calculated pair binding energy is its excessive magnitude: all the long-ranged deformation potential is simulated in the present model by the nearest-neighbor Koster-Slater field; hence the nearest-neighbor deformation should be overestimated at the expense of more distant deformations, and the calculated binding energy of nearest-neighbor pairs should be too large. The success of the model for the NN_1 pair energy and for the isolated nitrogen energy ($NN_\infty \equiv N_x \equiv A$) implies that the intermediate-distance pairs should also be fairly well described by the model. However, it is doubtful that a quantitative description of all the NN_1 pair binding energies is possible unless one treats the lattice deformation realistically and handles the symmetry of the trap potential properly.⁴⁵

B. Intensities

1. Dependence on x

The probabilities $|\langle B(0) | \psi \rangle|^2$ that the N_Γ and N_x states are in a Bloch state of zero wave vector are given in Fig. 6 as functions of alloy composition x . If N_Γ and N_x were occupied and if there were no radiationless transitions, these probabilities would be proportional to the observed luminescence intensities of the lines N_Γ and N_x (See Fig. 7). The computed ratio of the N_Γ to N_x intensities (at saturation photoexcitation) is given in Fig. 8. A quantitative comparison of Fig. 8 with the data of Fig. 7 is not appropriate because the data are for different alloys and varying experimental conditions; nevertheless two qualitative features of the data can be compared with the theory: (i) the N_Γ luminescence is generally comparable with or weaker than the N_x luminescence intensity; and (ii) the $N_\Gamma:N_x$ intensity ratio has a maximum near $x \approx 0.37$. The computed N_Γ intensity is almost two orders of magnitude larger than the N_x intensity; this is likely due to the fact that the computations do not include radiationless tran-

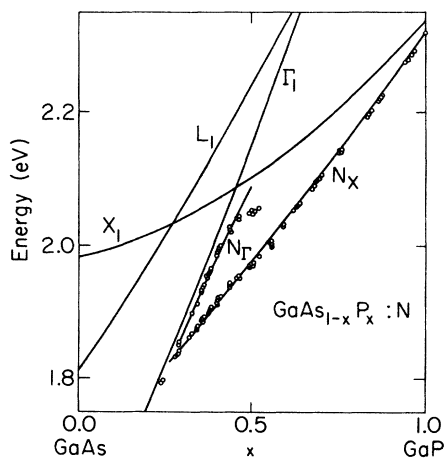


FIG. 5. Computed energy levels for the N_Γ and N_x states, compared with experimental data for the corresponding photoluminescence peaks.

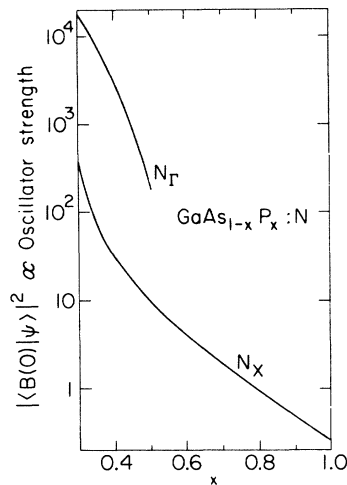


FIG. 6. Computed probabilities $|\langle B(0)|\psi\rangle|^2$, which are proportional to the oscillator strengths, for N_Γ and N_x . For alloy composition $x \geq 0.52$, N_Γ merges with the X_1 continuum for the theory presented here. Experimentally N_Γ is not observed in this range or merges with the weak $N_{\Gamma-x}$ emission.

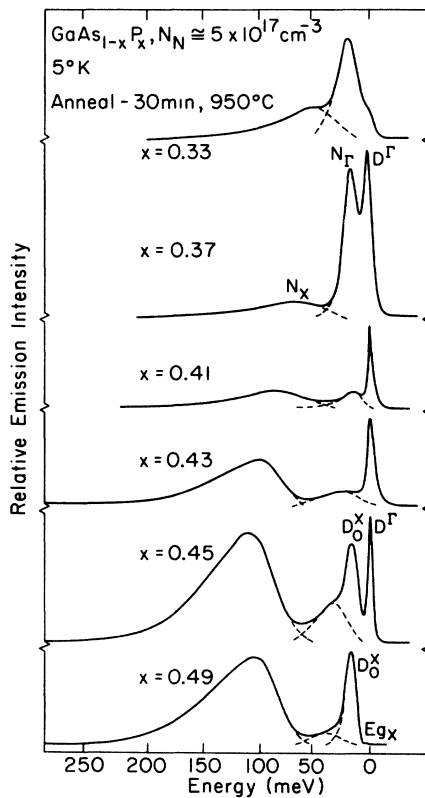


FIG. 7. Emission spectra at saturation photoexcitation for various alloy compositions. Note that the $N_\Gamma:N_x$ intensity ratio peaks near $x \approx 0.37$.

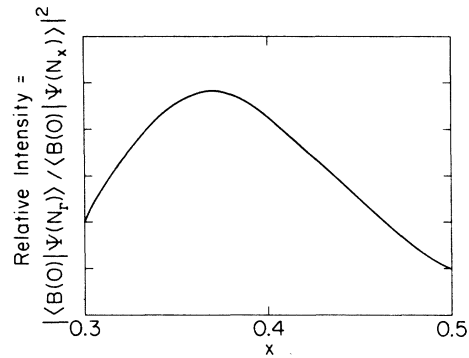


FIG. 8. Relative $N_\Gamma:N_x$ photoluminescence intensity as computed from Fig. 6 for $0.30 \leq x \leq 0.50$.

sitions, and the strength of the N_Γ line relative to N_x should be weakened by the larger cross section for radiationless decay expected for the less tightly bound, larger-radius N_Γ state. If the radiationless transition rates are not strong functions of composition x , the computed and measured $N_\Gamma:N_x$ ratios should exhibit similar x dependences; Figs. 7 and 8 show that this is the case, with the maximum ratio occurring near $x = 0.37$.

2. Pressure dependence

The composition dependence of the emission strengths can be compared with pressure-dependent luminescent intensities, provided the application of pressure is equivalent to an increase of alloy phosphorus content. Of course, an exact equivalence does not exist, but the physical picture outlined here attributes a major fraction of the changes in nitrogen's potential to lattice distortions, and hence an approximate relation between composition and pressure should hold. Nelson *et al.*^{5,51,52} have estimated $dx/dp \approx 0.011$ (kbar)⁻¹; employing this number, we have obtained the logarithmic derivatives of Table III and find much better agreement with pressure data than one would expect for such a simplified model.

C. Lifetimes $\tau(x)$

In Fig. 9 we display the computed lifetime τ of the N_x state as a function of alloy composition x , and compare it with the measurements of Chevalier *et al.*¹⁰ The computations assume that $\tau(x)$ is inversely proportional to $|\langle B(0)|\psi_{N_x}\rangle|^2$, with the proportionality constant fixed by the GaP ($x=1$) datum.⁵³ The agreement is quite satisfactory, with both theory and experiment being well approximated by $\tau = \tau_0 e^{\alpha x}$, with $\alpha_{\text{theor}} = 7.0$ being comparable with the experimental value $\alpha_{\text{exp}} = 2.9$.

TABLE III. Logarithmic derivatives of the N_x -luminescence intensities I with respect to alloy composition x and pressure p .

x	Theor.		Expt.
	$\frac{1}{I} \frac{dI}{dx}$ (in kbar $^{-1}$)	$\frac{1}{I} \frac{dI}{dp}$	$\frac{1}{I} \frac{dI}{dp}$ (in kbar $^{-1}$)
0.32 (N_x)	-34.1	-0.37	-0.39 ^a
0.48 (N_Γ)	-30.4	-0.33	-0.37 ^b
0.68 (N_x)	-7.8	-0.09	-0.05 ^b

^a Deduced from Ref. 51.

^b Deduced from Ref. 52.

V. SUMMARY

In summary we find that the semiphenomenological model provides a simple yet accurate description of the nitrogen trap in GaAs $_{1-x}$ P $_x$ (and probably in other ternary semiconducting alloys as well^{54,55}). The model accurately obtains the energies of the observed N_Γ and N_x luminescence lines and their dependences on alloy composition x ; it also produces good semiquantitative agreement with the observed energy of the NN $_1$ pair state in GaP. In the alloy GaAs $_{1-x}$ P $_x$, the model accounts for the observed luminescence intensities of the lines N_Γ and N_x and their dependences on pressure and alloy composition x .

The basic physical ideas underlying this model of GaAs $_{1-x}$ P $_x$ are that as the GaP mole fraction x is increased, (i) the lattice distortions and the ionicity and electronegativity differences (which determine the strength and the range of the impurity potential) weaken, and (ii) the virtual crystal density of states moves to higher energy. These two effects cause the principal nitrogen-trap level N_x to move to higher energy and to become less tightly bound relative to the X_1 -band edge. The nonzero range of the nitrogen potential permits it

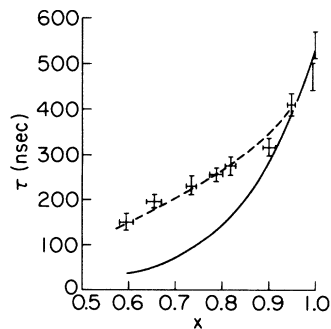


FIG. 9. Computed N_x radiative lifetime $\tau(x)$ compared with experimental data of Chevallier *et al.* (Ref. 10).

to bind a second exciton state N_Γ in direct-band-gap alloys.

In other work we shall show that these ideas have general applicability to isoelectronic traps in III-V alloys, and concepts arising from this study can be extended to other deep-level impurities.

ACKNOWLEDGMENTS

We would like to thank Professor M. Altarelli, Dr. T. N. Morgan, and Professor J. P. Wolfe for many helpful discussions. One of us (J.D.D.) acknowledges the support of the University of Illinois Center for Advanced Study.

APPENDIX A: ANALYSIS OF THE TWO-MINIMA APPROXIMATION

The model employed by Aspnes *et al.*²² is based on the Koster-Slater Schrödinger equation for the bound N_x state $|\psi(N_x)\rangle$:

$$[E(N_x) - E(\vec{k})] \langle B(\vec{k}) | \psi(N_x) \rangle = V \sum_{\vec{k}'} \langle B(\vec{k}') | \psi(N_x) \rangle, \quad (\text{A1})$$

where \vec{k} and \vec{k}' lie within the first Brillouin zone. Those authors approximated the solution to Eq. (A1) by neglecting diagonal coupling ($V=0$, when $k'=k$) and by solving the special case of only two important energies $E(k)$, namely those of the X - and L -band minima. They found

$$E(N_x) = \frac{1}{2}(E_X + E_L) - \frac{1}{2}[(E_X - E_L)^2 + 4V^2]^{1/2}, \quad (\text{A2})$$

where E_X and E_L are the X - and L -band edges, respectively, and V is a constant (independent of composition) interaction strength fixed by fitting 77-K GaAs $_{1-x}$ P $_x$:N luminescence data for $E(N_x)$ at $x \approx 0.30$.

The exact solution of the model is⁴⁷

$$\sum_{\vec{k}} \langle B(\vec{k}) | \psi(N_x) \rangle = V \sum_{\vec{k}} [E(N_x) - E(\vec{k})]^{-1} \times \sum_{\vec{k}'} \langle B(\vec{k}') | \psi(N_x) \rangle \quad (\text{A3})$$

or

$$1 = V \int_{-\infty}^{\infty} \rho(E') [E(N_x) - E']^{-1} dE', \quad (\text{A4})$$

where the density of states is

$$\rho(E') = \sum_{\vec{k}} \delta(E' - E(\vec{k})). \quad (\text{A5})$$

To recover the two-minima approximation one must (i) replace the actual density of states by two

δ functions (Fig. 10)

$$\rho(E')_{\text{Aspnes}} = \delta(E' - E_L) + \delta(E' - E_X), \quad (\text{A6})$$

and (ii) neglect diagonal coupling, i.e., replace

$$E(N_X) \rightarrow E(N_X)_{\text{Aspnes}} + V. \quad (\text{A7})$$

Neither of these approximations is tenable.

One feature of the exact solution, Eq. (A4), is that the N_X energy does not depend on details of the band structure, but only on an integral over the density of states. Hence the variation of the N_X energy with alloy composition in $\text{GaAs}_{1-x}\text{P}_x$ should not be cited as evidence supporting one band structure over another, when the competing band structures have similar densities of states. Even when the densities of states are somewhat different (as for the L and X minima in $\text{GaAs}_{1-x}\text{P}_x$; see Fig. 10), a more quantitative analysis than the two-minima approximation is required before the alloy dependence of $E(N_X)$ can be said to support one particular model.

The positions of the N_X line computed both with and without the L band and in the two-minima approximation, Eq. (A6), are given in Fig. 11 together with liquid-helium-temperature photoluminescence data from our nitrogen implantation studies. In all cases the values of V have been fixed by $x \approx 0.30$ data (following Aspnes *et al.*); when the L band was dropped, the density of states was re-normalized to be consistent with the requirements

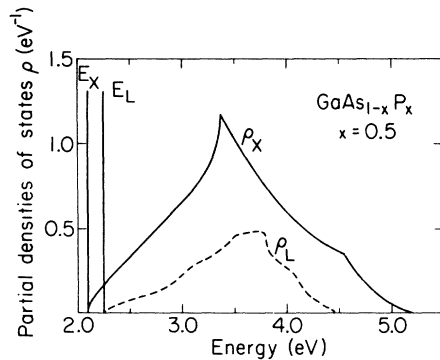


FIG. 10. Partial densities of states ρ associated with regions L (ρ_L) and X (ρ_X) as computed at $x=0.5$ by the empirical pseudopotential method within the virtual-crystal approximation. The two regions L and X carry a relative weight of approximately one to three and the corresponding density of states for the region Γ (ρ_Γ) is two orders of magnitude smaller and negligible on the scale indicated. The edge positions E_L and E_X are those computed from Eqs. (F3)–(F5) of Appendix F. The two-minima approximation of Aspnes *et al.* (Ref. 22) corresponds to replacing the two densities of states ρ_L and ρ_X by two δ functions of equal weight at E_L and E_X (vertical bars).

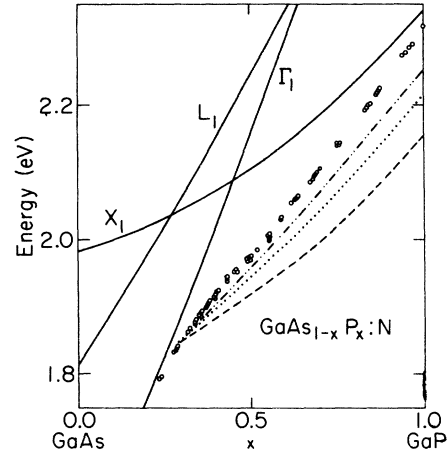


FIG. 11. Computed energy levels for the state N_X with a constant, composition-independent strength J fixed empirically at $x \approx 0.30$ according to (a) the two-minima model of Aspnes *et al.* (chain line); (b) exact solution with all three regions Γ , L , and X taken into account (dotted line); and (c) similar to (b) but with the L density of states ρ_L removed (dashed line).

of particle conservation

$$\int_{-\infty}^{\infty} \rho(E) dE = N.$$

Although Aspnes *et al.* found marginal agreement with fitting the parameters of their model to the Nelson *et al.*⁵ 77-K data (e.g., the predicted binding energy of the GaP A line is an order of magnitude too large), agreement with our 5-K spectra is generally poor (see Fig. 11). A comparison independent of the differences between reported ternary alloy data is afforded by fitting all parameters to the well-known GaP A-line energy (Fig. 12). The

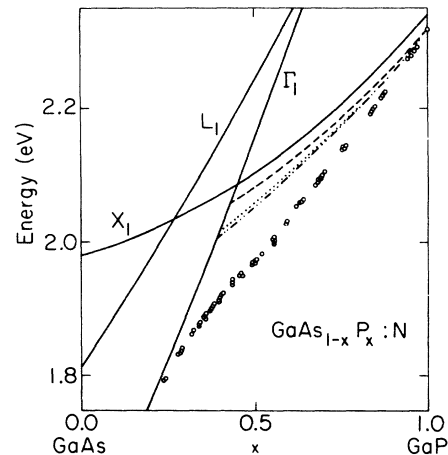


FIG. 12. Same as Fig. 11 except the constant, composition-independent strength J is now determined at the GaP limit ($x=1.0$).

curves in Fig. 12 show that a composition-independent V is inadequate; that the role of the L minima is not major, and that even the exact solution of the Aspnes model does not reproduce the observed dependence of $E(N_x)$ on x .

The Koster-Slater model with a constant interaction²⁰ V and a density of states $\rho(E)$ which shifts rigidly as a function of composition x produces a constant nitrogen binding energy [see Eq. (A4)]. A realistic density of states has relatively rigid principal features associated with the Γ , X , and L minima which shift in energy as x is varied; nevertheless such a density of states inserted into Eq. (A4) cannot reproduce the observed N_x energy unless V varies with composition (see Figs. 11 and 12). Moreover, the one-band, one-site Koster-Slater model produces at most one bound state,²⁵ and therefore cannot explain the occurrence of N_Γ . Hence a multisite composition-dependent potential is required.

APPENDIX B: COMPARISON WITH RECENT WORK OF KLEIMAN *et al.*

In recent work Kleiman *et al.*²³ have proposed a theory of the nitrogen trap based upon the 77-K alloy composition diagram of Nelson *et al.*⁵ (Fig. 4 of Ref. 5). It is difficult to compare details of the 5-K results of Fig. 1 with these higher-temperature data, because of thermal broadening and shifts in peak positions which occur at 77 K. Line fits to the 5-K data¹ indicate some shift in the N_x emission band peak to lower energy as x is decreased from unity, a consequence of increased phonon participation. It is likely that this effect

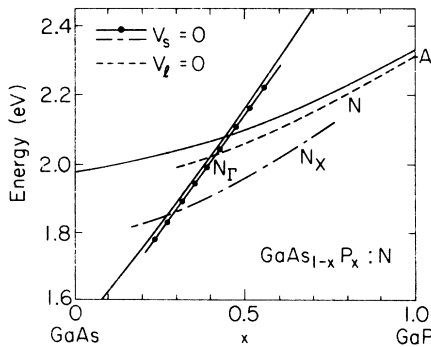


FIG. 13. Schematic plot (after Ref. 23) of the Kleiman *et al.* model for the isolated N trap in $\text{GaAs}_{1-x}\text{P}_x$. In this model, N_x is associated with the long-ranged strain tail of the potential alone and does not become the A line of GaP:N . An additional state (termed N), shallower than N_x , is assumed bound by the deep central cell potential for $x \geq 0.45$, and is traceable in theory to the A line of GaP:N . These assignments are to be contrasted with our liquid-helium-temperature data which showed that N_x evolves continuously from the A line of GaP and that N_Γ is the only prominent state shallower than N_x .

is even more dramatic in Fig. 4 of Ref. 5, accounting for the reported nonlinear dependence of the N_x peak on x .

Apart from such differences in the data, the interpretation of the origin of luminescence from the nitrogen trap by Kleiman *et al.* differs from that presented here. Their deeply bound N_x line is associated with a long-ranged strain tail of the potential (see Fig. 13), whereas we associate it with the central potential, due to local lattice distortion and the short-ranged electronegativity difference effect, as for the A line in GaP . The major feature of the model presented here is that N_x in the alloy and the A line in GaP have the same origin. In the theory of Kleiman *et al.* an additional electron state N is associated with the short-ranged central-cell potential, although its binding energy with respect to the X_1 minima is less than that of their long-ranged state N_x . As a result, the relationship of the states N and N_x in the ternary to the A line in the binary limit is not clear in the Kleiman theory. Finally the Kleiman calculations²³ predict an exceedingly small zone-center probability density for the N_x state whenever $x \geq 0.5$, a fact that seems difficult to reconcile with the observation of strong yellow-green N_x luminescence from diodes made of these materials.¹⁹

APPENDIX C: ONE OR TWO NITROGEN CENTERS?

Let us assume, for the moment, that the N_Γ and N_x states are due to two different nitrogen centers separated from each other by a distance \vec{R} (in Bohr radii a_B) and that each is a local ground state. Within the effective-mass theory of Luttinger and Kohn,³⁹ the wave functions for N_Γ and N_x are given by

$$\langle \vec{r} | \Psi(N_\Gamma) \rangle = \psi_\Gamma(\vec{r}) \langle \vec{r} | B(\vec{k}=0) \rangle = \psi_\Gamma(\vec{r}) u(\vec{k}=0, \vec{r}) \quad (\text{C1})$$

and

$$\begin{aligned} \langle \vec{r} | \Psi(N_x) \rangle &= \psi_x(\vec{r}) \langle \vec{r} | B(\vec{k}=\vec{k}_x) \rangle \\ &= \psi_x(\vec{r}) e^{i\vec{k}_x \cdot \vec{r}} u(\vec{k}=\vec{k}_x, \vec{r}), \end{aligned} \quad (\text{C2})$$

where $\psi_\Gamma(\vec{r})$ and $\psi_x(\vec{r})$ are envelope functions and $u(\vec{k}, \vec{r})$ is the periodic part of the host Bloch function $\langle \vec{r} | B(\vec{k}) \rangle$. For ground states, the envelope functions can be approximated by

TABLE IV. Values of $\sum_{\vec{g}} |a_{\vec{g}}|$ for $\text{GaAs}_{1-x}\text{P}_x$ at the anion site according to the virtual-crystal approximation and the empirical pseudopotential method.

x	$\sum_{\vec{g}} a_{\vec{g}} $
0.0	6.01
0.5	5.95
1.0	5.90

$$\psi_i(\vec{r}) \simeq [(\Delta E_i)^{3/4}/\pi^{1/2}]e^{-(\Delta E_i)^{1/2}r} \quad (\text{C3})$$

where $\Delta E_i = E(N_i) - E_i$, with $i = \Gamma$ or X ; E_i is the energy of the i th band edge in rydbergs while $E(N_i)$ is the energy of the N_i state. The overlap integral is

$$\begin{aligned} \langle \Psi(N_\Gamma) | \Psi(N_X) \rangle &= \int d\vec{r} e^{i\vec{k}_X \cdot \vec{r}} u^*(k=0, r) \\ &\quad \times u(k=\vec{k}_X, r) \psi_\Gamma^*(\vec{r}) \psi_X(\vec{r}) \\ &= \sum_{\vec{G}} a_{\vec{G}} \int d\vec{r} e^{i(\vec{G} + \vec{k}_X) \cdot \vec{r}} \psi_\Gamma^*(\vec{r}) \psi_X(\vec{r}), \end{aligned} \quad (\text{C4})$$

where the last line is obtained from the previous one by expanding the periodic function $u^*(\vec{k}=0, \vec{r}) \times u(\vec{k}=\vec{k}_X, \vec{r})$ (with periodicity of the host lattice) in a Fourier series of the reciprocal-lattice vectors \vec{G} . In general, we obtain

$$|\langle \Psi(N_\Gamma) | \Psi(N_X) \rangle| \leq \left(\sum_{\vec{G}} |a_{\vec{G}}| \right) \int d\vec{r} |\psi_\Gamma^*(\vec{r}) \psi_X(\vec{r})|, \quad (\text{C5})$$

where the prefactor $\sum_{\vec{G}} |a_{\vec{G}}|$ is found to be ~ 6 (Table IV) when calculated by the empirical pseudopotential method³⁸ within the virtual-crystal approximation.¹⁵ Therefore we estimate the overlap integral by

$$\begin{aligned} |\langle \Psi(N_\Gamma) | \Psi(N_X) \rangle| &< 7 \int d\vec{r} \psi_\Gamma(\vec{r}) \psi_X(\vec{r}) \\ &= \frac{7}{\pi} (\Delta E_\Gamma \Delta E_X)^{3/4} \int d\vec{r} e^{-(\Delta E_\Gamma)^{1/2}r} e^{-(\Delta E_X)^{1/2}|\vec{r}-\vec{R}|}, \end{aligned} \quad (\text{C6})$$

which is a well-known two-center integral that can be integrated analytically by transforming into the prolate spheroidal coordinates.^{56, 57} The final result is

$$\begin{aligned} |\langle \Psi(N_\Gamma) | \Psi(N_X) \rangle| &= (28/A |B|) (\Delta E_\Gamma \Delta E_X)^{3/4} \\ &\quad \times (\frac{1}{2}R)^3 e^{-(A+B)} (A^{-1} + A^{-2} + |B|^{-1} - B^{-2}), \end{aligned} \quad (\text{C7})$$

where

$$A = \frac{1}{2} [(\Delta E_\Gamma)^{1/2} + (\Delta E_X)^{1/2}] R$$

and

$$B = \frac{1}{2} [(\Delta E_\Gamma)^{1/2} - (\Delta E_X)^{1/2}] R.$$

Assuming that

$$R = 200 \text{ \AA} = 378 a_B,$$

$$\Delta E_\Gamma = 20 \text{ meV} = 3.84 \times 10^{-2} \text{ Ry},$$

and

$$\Delta E_X = 90 \text{ meV} = 8.14 \times 10^{-2} \text{ Ry},$$

we estimate the overlap integral to be less than 1.38×10^{-5} . We note here that the average separa-

tion between nitrogens is at most 300 \AA for a peak implanted concentration of 10^{17} cm^{-3} , and that ΔE_X is considerably larger than 90 meV for the composition range $0.28 \leq x \leq 0.45$ in which N_Γ and N_X coexist. The estimated value for the overlap integral 1.4×10^{-5} is hence a very liberal upper bound for 10^{17} cm^{-3} ; more careful estimates show that this upper bound holds for typical nitrogen concentrations of 10^{16} – 10^{18} cm^{-3} . The rate τ for decay of N_Γ into N_X can now be estimated by the ‘‘golden rule’’:

$$\tau^{-1} \cong \tau_0^{-1} |\langle \Psi(N_\Gamma) | \Psi(N_X) \rangle|^2 \leq 1.9 \times 10^{-10} \tau_0^{-1}, \quad (\text{C8})$$

where τ_0 is a characteristic time which should not be shorter than the conduction-band thermalization time of $\sim 10^{-13} \text{ sec}$. Hence we conclude that the $N_\Gamma \rightarrow N_X$ transfer rate for a two-nitrogen-center model is no faster than $0.5 \times 10^{-3} \text{ sec}$ and is very slow compared with typical radiative lifetimes of 10^{-6} – 10^{-9} sec . Direct transfer between N_Γ and N_X states in this model is therefore forbidden at low nitrogen concentration (say, 10^{17} cm^{-3}).

Likewise, resonant transfer is also forbidden, since the average separation between nitrogens (300 \AA for a concentration of 10^{17} cm^{-3}) is much greater than the distance of 100 \AA for effective tunneling reported by Wiesner *et al.*⁵⁸ in GaP. In conclusion, we rule out the two-center model for the observed N_Γ and N_X lines because it predicts that N_Γ and N_X lines should have comparable intensities at low nitrogen concentrations and low excitation levels, contrary to experimental observations (Figs. 3 and 4).

APPENDIX D: ARGUMENT THAT A, STATES ARE MOST LIKELY TO BE BOUND

In the notation of Appendix E the matrix elements of the potential are

$$\langle 0 | V | 0 \rangle = -J, \quad \langle 0 | V | 1 \rangle = -b,$$

$$\langle 1 | V | 1 \rangle = -L$$

$$= V(0) + 2V(2) + 2V'(2) + 2V(4) + 4V(6) + V(8),$$

$$\langle E, m, 1, 1 | V | E, m, 1, 1 \rangle$$

$$= V(0) - V(2) - V'(2) + 2V(4) - 2V(6) + V(8), \quad m = 1, 2,$$

$$\langle T_1, m, 1, 1 | V | T_1, m, 1, 1 \rangle$$

$$= V(0) - V(2) - V'(2) + 2V(6) - V(8), \quad m = 1, 2, 3,$$

$$\langle T_2, m, 1, 1 | V | T_2, m, 1, 1 \rangle$$

$$= V(0) + V(2) + V'(2) - 2V(6) - V(8), \quad m = 1, 2, 3,$$

$$\langle T_2, m, 2, 1 | V | T_2, m, 2, 1 \rangle = V(0) - 2V(4) + V(8),$$

$$m = 1, 2, 3,$$

$$\langle T_2, m, 1, 1 | V | T_2, m, 2, 1 \rangle = \sqrt{2} [V(2) - V'(2)],$$

$$m = 1, 2, 3, \quad (\text{D1})$$

where

$$V(4|\vec{R}_i - \vec{R}_j|^2/a_L^2) = \langle W(\vec{R}_i) | V | W(\vec{R}_j) \rangle. \quad (\text{D2})$$

For $i = 2$, the above definition of $V(i)$ is not unique, and two parameters $V(2)$ and $V'(2)$ are defined, where $V(2)$ is the parameter for configurations such that a Ga-ion site lies between \vec{R}_i and \vec{R}_j in the same plane and $V'(2)$ is for the other configuration.

All the coefficients $V(i)$ have the same sign for monotonic potentials. Hence Eqs. (D1) indicate a great deal of cancellation for matrix elements of V between states of E , T_1 , and T_2 symmetry.⁴⁶ No such cancellation occurs for A_1 symmetry. Physically, only A_1 (s -like) electrons make significant contact with the strong central-cell potential; hence these states are most likely to be bound by a short-ranged potential.

APPENDIX E: MATRIX ELEMENTS OF $(E - H_0)^{-1}V$ AND WAVE FUNCTIONS

Matrix elements of $(E - H_0)^{-1}V$

Evaluation of matrix elements of the operator $(E - H_0)^{-1}V$ is facilitated by replacing each cell index i with two labels, the shell index s (which labels the shell of cells all equidistant from the central nitrogen impurity) and the cell index σ_s (which labels each of the n_s cells in the s th shell). Then the potential, Eq. (1), is

$$V = \sum_{s, s'=0}^1 \sum_{\sigma}^{n_s} \sum_{\sigma'}^{n_{s'}} |W(\vec{R}_{s, \sigma})\rangle V_{s\sigma, s'\sigma'} \langle W(\vec{R}_{s', \sigma'})|. \quad (\text{E1})$$

The conduction-band Wannier functions of a particular shell form a basis for a reducible representation of T_d , the symmetry group of H_0 . The calculations are simplified by performing a unitary

transformation to basis functions which transform according to the m th row of the l th irreducible representation. In general the s th shell may have n different linear combinations of Wannier functions which transform according to the m th row of the l th irreducible representation (because the reducible representation may contain various irreducible representations more than once); the relevant transformation coefficients (for $s = 1$)

$$\langle W(\vec{R}_{s, \nu}) | l m n s \rangle$$

are given in Table V. With this transformation the potential becomes

$$V = \sum_{s, s'=0}^1 \sum_{l, m}^{l, m} |l m n s\rangle \langle l m n s | V | l' m' n' s' \rangle \langle l' m' n' s'|. \quad (\text{E2})$$

The assumption that V has T_d symmetry causes $\langle l m n s | V | l' m' n' s' \rangle$ to vanish unless $l = l'$ and $m = m'$ (for unitary representations). For either the central or the first shell ($s = 0, 1$), only one basis function ($n = 1$) transforms according to $A_1 (= lm)$ and we write A_1 for lmn . To establish a connection with conventional notation and that of Eqs. (8a) and (8b), we write

$$\begin{aligned} \langle A_1 0 | V | A_1 0 \rangle &\equiv -J = \langle 0 | V | 0 \rangle, \\ \langle A_1 0 | V | A_1 1 \rangle &\equiv -b = \langle 0 | V | 1 \rangle, \\ \langle A_1 1 | V | A_1 1 \rangle &\equiv -L = \langle 1 | V | 1 \rangle, \end{aligned} \quad (\text{E3})$$

in which case V becomes

$$V = -J |0\rangle \langle 0| - L |1\rangle \langle 1| - b |0\rangle \langle 1| - b^* |1\rangle \langle 0| + V_{\text{other}}, \quad (\text{E4})$$

where V_{other} contains contributions to Eq. (E2) with s and s' equal to unity, and with l equal to irreduc-

TABLE V. Transformation matrix $\langle l m n s | W(\vec{R}_\nu, s) \rangle$ for the first shell ($s = 1$). \vec{R}_ν is represented by its Cartesian components and is in units of $\frac{1}{2}a_L$, where a_L is the lattice constant of the virtual crystal.

$\langle l m n 1 $	$W(\vec{R}_\nu)$												α
	$\vec{R}_\nu \equiv (110)$	$(\bar{1}\bar{1}0)$	$(\bar{1}10)$	$(1\bar{1}0)$	(011)	$(0\bar{1}\bar{1})$	$(0\bar{1}1)$	$(01\bar{1})$	(101)	$(10\bar{1})$	$(\bar{1}01)$	$(\bar{1}0\bar{1})$	
$\langle A_1 111 $	α	α	α	α	α	α	α	α	α	α	α	α	$(12)^{-1/2}$
$\langle E 111 $	0	0	0	0	α	α	α	α	$-\alpha$	$-\alpha$	$-\alpha$	$-\alpha$	$(8)^{-1/2}$
$\langle E 211 $	2α	2α	2α	2α	$-\alpha$	$-\alpha$	$-\alpha$	$-\alpha$	$-\alpha$	$-\alpha$	$-\alpha$	$-\alpha$	$(24)^{-1/2}$
$\langle T_1 111 $	α	α	$-\alpha$	$-\alpha$	0	0	0	0	$-\alpha$	$-\alpha$	α	α	$(8)^{-1/2}$
$\langle T_1 211 $	$-\alpha$	α	$-\alpha$	α	α	α	$-\alpha$	$-\alpha$	0	0	0	0	$(8)^{-1/2}$
$\langle T_1 311 $	0	0	0	0	$-\alpha$	α	$-\alpha$	α	α	$-\alpha$	α	$-\alpha$	$(8)^{-1/2}$
$\langle T_2 111 $	α	α	$-\alpha$	$-\alpha$	0	0	0	0	α	α	$-\alpha$	$-\alpha$	$(8)^{-1/2}$
$\langle T_2 211 $	α	$-\alpha$	α	$-\alpha$	α	α	$-\alpha$	$-\alpha$	0	0	0	0	$(8)^{-1/2}$
$\langle T_2 311 $	0	0	0	0	α	$-\alpha$	α	$-\alpha$	α	$-\alpha$	α	$-\alpha$	$(8)^{-1/2}$
$\langle T_2 121 $	0	0	0	0	α	$-\alpha$	$-\alpha$	α	0	0	0	0	$(4)^{-1/2}$
$\langle T_2 221 $	0	0	0	0	0	0	0	0	α	$-\alpha$	$-\alpha$	α	$(4)^{-1/2}$
$\langle T_2 321 $	α	$-\alpha$	$-\alpha$	α	0	0	0	0	0	0	0	0	$(4)^{-1/2}$

ible representations other than A_1 . Appendix D shows that matrix elements involving V_{other} are not germane. Since H_0 has T_d symmetry, the symmetrized Wannier functions $|lmns\rangle$ partially diagonalize the operator $(E - H_0)^{-1}$, and we have identities such as

$$\begin{aligned} \langle A_1 0 | (E - H_0)^{-1} &\equiv \sum_{lmns} \langle A_1 0 | (E - H_0)^{-1} | lmns \rangle \langle lmns | \\ &= \sum_{s=0}^{\infty} \langle A_1 0 | (E - H_0)^{-1} | A_1 s \rangle \langle A_1 s | . \end{aligned} \quad (\text{E5})$$

The potential has a range $s \leq 1$; hence the secular equation (9) assumes the simple form

$$\begin{vmatrix} 1 + \langle 0 | G | 0 \rangle J + \langle 0 | G | 1 \rangle b^* & \langle 0 | G | 0 \rangle b + \langle 0 | G | 1 \rangle L \\ \langle 1 | G | 0 \rangle J + \langle 1 | G | 1 \rangle b^* & 1 + \langle 1 | G | 0 \rangle b + \langle 1 | G | 1 \rangle L \end{vmatrix} = 0, \quad (\text{E6})$$

where we have

$$G \equiv (E - H_0)^{-1}. \quad (\text{E7})$$

The secular equation becomes

$$\begin{aligned} (1 + \langle 0 | G | 0 \rangle J)(1 + \langle 1 | G | 1 \rangle L) \\ = \langle 1 | G | 1 \rangle \langle 0 | G | 0 \rangle |b|^2 + (JL - |b|^2) \\ \times \langle 0 | G | 1 \rangle \langle 1 | G | 0 \rangle - \langle 0 | G | 1 \rangle b^* - \langle 1 | G | 0 \rangle b. \end{aligned} \quad (\text{E8})$$

Concentrating on the off-diagonal matrix element $b = -\langle 0 | V | 1 \rangle$ involving the overlap of Wannier functions in different cells (therefore having a considerably smaller magnitude than the single-cell matrix elements J and L), we note that our calculations (Appendix F) find for all the energies of interest in the range $x \geq 0.28$

$$\left| \frac{\langle 0 | G | 1 \rangle \langle 1 | G | 0 \rangle}{\langle 0 | G | 0 \rangle \langle 1 | G | 1 \rangle} \right| \leq 0.02. \quad (\text{E9})$$

Hence we are justified in making the local approximation: neglecting the right-hand side of Eq. (E8). This leaves the model with two adjustable parameters instead of three—a desirable simplification. The resulting eigenvalue equations are

$$\langle 0 | G [E(N_x)] | 0 \rangle = -1/J \quad (\text{E10})$$

and

$$\langle 1 | G [E(N_r)] | 1 \rangle = -1/L. \quad (\text{E11})$$

The numerical evaluation of the matrix elements of $G = (E - H_0)^{-1}$ is discussed in Appendix F.

TABLE VI. Character table of reducible representations generated by A_1 conduction-band Wannier functions centered at anion sites in a shell equidistant to the impurity site. Each shell and its associated reducible representation are characterized by three positive integers $\langle \mu, \nu, \lambda \rangle$ such that $\mu \geq \nu \geq \lambda \geq 0$ and that $(\mu + \nu + \lambda)$ is even. Decomposition of each $\langle \mu, \nu, \lambda \rangle$ representation into reducible ones of the T_d group (Table II) is given and the number n of A_1 states appearing in the $\langle \mu, \nu, \lambda \rangle$ representation listed.

Representation	E	$3C_4^2$	$6S_4$	$6\sigma_d$	$8C_3$	Decomposition	n
$\langle 0, 0, 0 \rangle$	1	1	1	1	1	A_1	1
$\langle 2\mu, 0, 0 \rangle$	6	2	0	2	0	$A_1 + E + T_2$	1
$\langle 2\mu, 2\mu, 2\mu \rangle$	8	0	0	4	2	$2A_1 + 2T_2$	2
$\langle \mu, \mu, 0 \rangle$	12	0	0	2	0	$A_1 + E + T_1 + 2T_2$	1
$\langle \mu, \mu, 2\lambda \rangle$ $\mu > 2\lambda \neq 0$	24	0	0	4	0	$2A_1 + 2E + 2T_1 + 4T_2$	2
$\langle 2\mu, \lambda, \lambda \rangle$ $2\mu > \lambda \neq 0$	24	0	0	4	0	$2A_1 + 2E + 2T_1 + 4T_2$	2
$\langle \mu, \nu, 0 \rangle$ $\mu > \nu \neq 0$	24	0	0	0	0	$A_1 + A_2 + 2E + 3T_1 + 3T_2$	1
$\langle \mu, \nu, \lambda \rangle$ $\mu > \nu > \lambda \neq 0$	48	0	0	0	0	$2A_1 + 2A_2 + 4E + 6T_1 + 6T_2$	2

Wave functions: direct space

The bound-state wave functions of energy E [$= E(N_X)$ or $E(N_\Gamma)$] are given by

$$|\psi\rangle = (E - H_0)^{-1} V |\psi\rangle \quad (\text{E12})$$

or

$$\begin{aligned} \langle A_1 n s | \psi \rangle &= \sum_{\substack{n' \nu \\ s' \sigma}} \langle A_1 n s | G | A_1 n' s' \rangle \\ &\times \langle A_1 n' s' | V | A_1 \nu \sigma \rangle \langle A_1 \nu \sigma | \psi \rangle. \end{aligned} \quad (\text{E13})$$

Here we have made use of the selection rules⁴⁶ which follow from the fact that G and V each are invariant under the operations of T_d . The form we have chosen for V [Eq. (E4)] further simplifies the expression for the wave function

$$\begin{aligned} -\langle A_1 n s | \psi \rangle &= [J \langle A_1 n s | G | 0 \rangle + b^* \langle A_1 n s | G | 1 \rangle] \langle 0 | \psi \rangle \\ &+ [b \langle A_1 n s | G | 0 \rangle + L \langle A_1 n s | G | 1 \rangle] \langle 1 | \psi \rangle. \end{aligned} \quad (\text{E14})$$

For simplicity, we omit the label A_1 ; moreover it can be shown⁵⁹ using Table VI that the label n can likewise be suppressed, because only the totally symmetric basis function ($n=1$) has nonzero matrix elements with $G|0\rangle$ or $G|1\rangle$:

$$\begin{aligned} \langle B(\vec{k}) | \psi(N_X) \rangle &= [E(N_X) - E(\vec{k})]^{-1} \left(\sum_{\vec{k}} [E(N_X) - E(\vec{k})]^{-2} \right)^{-1/2}, \\ \langle B(\vec{k}) | \psi(N_\Gamma) \rangle &= [E(N_\Gamma) - E(\vec{k})]^{-1} \sum_{i=1}^{12} e^{-i\vec{k} \cdot \vec{R}_i} \left(\sum_{\vec{k}} \sum_{i,j=1}^{12} e^{-i\vec{k} \cdot (\vec{R}_i - \vec{R}_j)} [E(N_\Gamma) - E(\vec{k})]^{-2} \right)^{-1/2}. \end{aligned} \quad (\text{E19})$$

These probability densities $|\langle B(\vec{k}) | \psi \rangle|^2$ for N_X and N_Γ are given in Figs. 14 and 15, respectively, for wave vectors \vec{k} in the (100) direction and for alloy compositions x near the direct-indirect crossover.

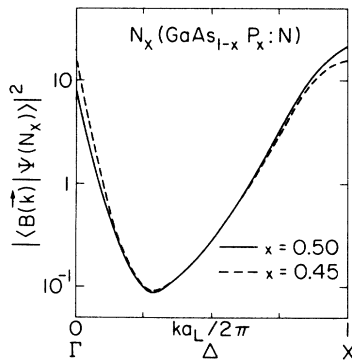


FIG. 14. Computed probability density $|\langle B(\vec{k}) | \psi(N_X) \rangle|^2$ for the N_X level as a function of \vec{k} in the (100) direction for $x=0.45$ (dashed) and $x=0.50$ (solid) in $\text{GaAs}_{1-x}\text{P}_x$.

$$|s\rangle = (n_s)^{1/2} \sum_{\sigma=1}^{n_s} |W(\vec{R}_{s,\sigma})\rangle = |A_1 s\rangle = |A_1 1s\rangle. \quad (\text{E15})$$

Hence we have

$$\begin{aligned} -\langle s | \psi \rangle &= [J \langle s | G | 0 \rangle + b^* \langle s | G | 1 \rangle] \langle 0 | \psi \rangle \\ &+ [b \langle s | G | 0 \rangle + L \langle s | G | 1 \rangle] \langle 1 | \psi \rangle, \end{aligned} \quad (\text{E16})$$

where the ratio $\langle 1 | \psi \rangle / \langle 0 | \psi \rangle$ is determined by solving the secular equation, and the coefficient $\langle 0 | \psi \rangle$ (or $\langle 1 | \psi \rangle$) is determined by the normalization condition

$$\sum_{s=0}^{\infty} \langle \psi | s \rangle \langle s | \psi \rangle = 1. \quad (\text{E17})$$

In the local approximation [see Eqs. (E8)–(E10)] this becomes

$$\langle s | \psi(N_X) \rangle = |J|^{-1} \langle s | G[E(N_X)] | 0 \rangle \{ \langle 0 | G^2[E(N_X)] | 0 \rangle \}^{-1/2} \quad (\text{E18})$$

$$\langle s | \psi(N_\Gamma) \rangle = |L|^{-1} \langle s | G[E(N_\Gamma)] | 1 \rangle \{ \langle 1 | G^2[E(N_\Gamma)] | 1 \rangle \}^{-1/2}.$$

Wave functions: reciprocal space

The k -space wave functions are easily obtained from the direct-space wave functions by Bloch transformation; in the local approximation this is

Figure 15 shows that the zone-boundary component of the wave function $\psi(N_\Gamma)$ increases considerably as the alloy composition is varied from $x=0.45$ to $x=0.50$; this increase is caused mainly by the approaching large X_1 density of states.

APPENDIX F: NUMERICAL EVALUATION OF MATRIX ELEMENTS OF $G \equiv (E - H_0)^{-1}$

In the notation of Appendix E, the matrix elements of G^n are

$$\begin{aligned} \langle s | G^n | s' \rangle &= (n_s n_{s'})^{-1/2} \\ &\times \sum_{\sigma=1}^{n_s} \sum_{\sigma'=1}^{n_{s'}} \sum_{\vec{k}} e^{i\vec{k} \cdot (\vec{R}_{s,\sigma} - \vec{R}_{s',\sigma'})} [E - E(\vec{k})]^{-n}. \end{aligned} \quad (\text{F1})$$

$\langle 0 | G^n | 0 \rangle$ is best evaluated by computing the density of states $\rho(E')$ employing standard technique⁶⁰ and integrating

$$\langle 0 | G^n | 0 \rangle = \int_{-\infty}^{\infty} \rho(E') (E - E')^{-n} dE'. \quad (\text{F2})$$

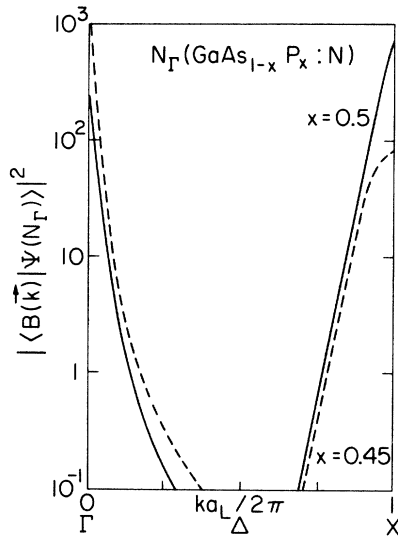


FIG. 15. Computed probability density $|\langle B(\vec{k})|\psi(N_\Gamma)\rangle|^2$ for the N_Γ level as a function of \vec{k} in the (100) direction.

The remaining integrals are evaluated using the special points method of Chadi and Cohen,⁶¹ employing 408 special points.

The energy band $E(\vec{k})$ and density of states $\rho(E)$ are obtained using the empirical pseudopotential method³⁸ in the virtual-crystal approximation¹⁵ for $\text{GaAs}_{1-x}\text{P}_x$. The relevant form factors $V_G(x)$ and lattice constants $a_L(x)$ are obtained by interpolation¹⁵ of those for GaAs and GaP.^{38,62}

In all cases the integrals in \vec{k} space are computed separately for each of three regions of the Brillouin zone²⁰:

$$\Gamma \text{ region: } 0 \leq k_i a_L / 2\pi \leq 0.125;$$

$$L \text{ region: } 0.125 \leq k_i a_L / 2\pi \leq 0.5;$$

$$X \text{ region: } 0.5 \leq k_i a_L / 2\pi \text{ to zone boundary};$$

where $i = x, y, \text{ and } z$, and where $\vec{k} = (k_x, k_y, k_z)$.

When we first performed this calculation, we found (i) that we had neither accurately predicted

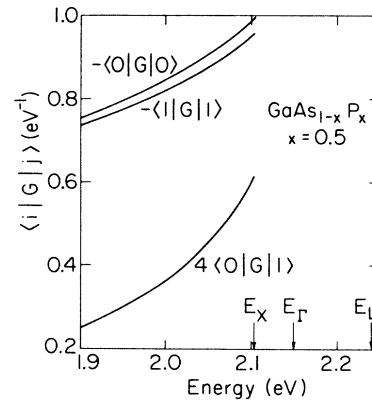


FIG. 16. Typical behavior of matrix elements of the Green's function $G = (E - H_0)^{-1}$. Vertical arrows indicate edge positions E_Γ , E_L , and E_X as computed from Eqs. (F3)–(F5) of Appendix F.

the energies of the conduction-band edges Γ , X , and L , nor their variation with composition x ; and (ii) that the contributions to $(E - H_0)^{-1}$ from the three Brillouin-zone regions had not significantly changed their *shapes* (as a function of E) when x had been varied from zero to unity. Therefore, to compensate for the inadequate edge positions, we computed contributions from the three regions of the Brillouin zone only for $x = \frac{1}{2}$ and rigidly shifted their energies until the thresholds coincided with the observed Γ -, L -, and X -band edges at⁶³ 4.2 K:

$$E(\Gamma) = (1.519 + 1.155x + 0.210x^2) \text{ eV}, \quad (\text{F3})$$

$$E(L) = (1.815 + 0.770x + 0.160x^2) \text{ eV}, \quad (\text{F4})$$

$$E(X) = (1.982 + 0.133x + 0.221x^2) \text{ eV}. \quad (\text{F5})$$

Typical examples of $\langle 0|G|0\rangle$, $\langle 0|G|1\rangle$, and $\langle 1|G|1\rangle$ are plotted as functions of E in Fig. 16. Note that $\langle 0|G|0\rangle$ and $\langle 1|G|1\rangle$ are of comparable magnitude throughout the energy range of interest, whereas $\langle 0|G|1\rangle$ is normally less than 15% as large.

*Research supported by the U.S. ERDA Contract No. ERDA-EY-76-C-02-1198.

†Research supported by the Joint Services Electronics Program (U.S. Army, U.S. Navy, and U.S. Air Force) under Contract No. DAAB-07-72-C-0259, and by Monsanto Co.

¹D. J. Wolford, B. G. Streetman, W. Y. Hsu, J. D. Dow, (unpublished). This article, paper I of the series, contains a summary of the data including those discussed in Refs. 2–7.

²D. J. Wolford, B. G. Streetman, R. J. Nelson and N. Holonyak, Jr., Appl. Phys. Lett. **28**, 711 (1976).

³D. J. Wolford, B. G. Streetman, R. J. Nelson, and N. Holonyak, Jr., Solid State Commun. **19**, 741 (1976).

⁴D. J. Wolford, B. G. Streetman, W. Y. Hsu, J. D. Dow, R. J. Nelson, and N. Holonyak, Jr., Phys. Rev. Lett. **36**, 1400 (1976).

⁵R. J. Nelson, N. Holonyak, Jr., J. J. Coleman, D. Lazarus, W. O. Groves, D. L. Keune, M. G. Craford, D. J. Wolford, and B. G. Streetman, Phys. Rev. B **14**, 685 (1976).

⁶D. J. Wolford, B. G. Streetman, W. Y. Hsu, and J. D. Dow, Thirteenth International Conference on the Physics of Semiconductors, Rome, 1976 (unpublished), p. 1049.

⁷D. J. Wolford, R. E. Anderson and B. G. Streetman, J. Appl. Phys. **48**, 2442 (1977).

⁸D. G. Thomas and J. J. Hopfield, Phys. Rev. **150**, 680 (1966).

- ⁹E. Cohen, M. D. Sturge, N. O. Lipari, M. Altarelli, and A. Baldereschi, *Phys. Rev. Lett.* **35**, 1591 (1975).
- ¹⁰J. Chevallier, H. Mariette, D. Diguët, and G. Poibland, *Appl. Phys. Lett.* **28**, 375 (1976).
- ¹¹M. H. Lee, N. Holonyak, Jr., J. C. Campbell, W. O. Groves, M. G. Craford, and D. L. Keune, *Appl. Phys. Lett.* **24**, 310 (1974); *J. Appl. Phys.* **45**, 1975 (1974).
- ¹²D. D. Sell, *Phys. Rev. B* **6**, 3750 (1972).
- ¹³P. J. Dean and D. G. Thomas, *Phys. Rev.* **150**, 690 (1966).
- ¹⁴A. Onton and L. M. Foster, *J. Appl. Phys.* **43**, 5084 (1972).
- ¹⁵See, for example, J. C. Phillips, *Bonds and Bands in Semiconductor* (Academic, New York, 1973), Chap. 8, p. 212.
- ¹⁶T. Kamiya and E. Wagner, *J. Appl. Phys.* **47**, 3219 (1976).
- ¹⁷M. G. Craford, R. W. Shaw, A. H. Herzog, and W. O. Groves, *J. Appl. Phys.* **43**, 4075 (1972), and references therein.
- ¹⁸N. Holonyak, Jr., R. D. Dupuis, H. M. Macksey, M. G. Craford, and W. O. Groves, *J. Appl. Phys.* **43**, 4148 (1972), and references therein.
- ¹⁹M. G. Craford and N. Holonyak, Jr., in *Optical Properties of Solids: New Developments*, edited by B. O. Seraphin (North-Holland, Amsterdam, 1975), Chap. 5.
- ²⁰D. R. Scifres, N. Holonyak, Jr., C. B. Duke, G. G. Kleiman, A. B. Kunz, M. G. Craford, W. O. Groves, and A. H. Herzog, *Phys. Rev. Lett.* **27**, 191 (1971); D. R. Scifres, H. M. Macksey, N. Holonyak, Jr., R. D. Dupuis, G. W. Zack, C. B. Duke, G. G. Kleiman, and A. B. Kunz, *Phys. Rev. B* **5**, 2206 (1972).
- ²¹M. Altarelli, *Phys. Rev. B* **11**, 5031 (1975).
- ²²D. E. Aspnes, C. G. Olson, and D. W. Lynch, *Phys. Rev. Lett.* **37**, 766 (1976); D. E. Aspnes, *Phys. Rev. B* **14**, 5331 (1976).
- ²³G. G. Kleiman, R. J. Nelson, N. Holonyak, Jr., and J. J. Coleman, *Phys. Rev. Lett.* **37**, 375 (1976); G. G. Kleiman, *Phys. Rev. B* **15**, 802 (1977).
- ²⁴G. F. Koster and J. C. Slater, *Phys. Rev.* **95**, 1167 (1954).
- ²⁵A graphical solution of Eq. (A4) produces at most one state below the lowest band edge.
- ²⁶H. Ehrenreich, *Phys. Rev.* **120**, 1951 (1960).
- ²⁷If the central-cell potential were unimportant in binding N_x , then one would expect that not only nitrogen but any electron-trapping center surrounded by a comparable strain field might produce states at least as deep as N_x and N_Γ .
- ²⁸Near $x \approx 0.5$ the N_Γ line becomes very weak and broad (Fig. 7); although its exact position becomes uncertain, $dE(N_\Gamma)/dx$ appears to decrease. Luminescence traceable from N_Γ in this region of the composition diagram has been labeled $N_{\Gamma-x}$. The $N_{\Gamma-x}$ luminescence is currently under study. One might speculate that part of the deepening of the $N_{\Gamma-x}$ level near the direct-indirect crossover ($x \approx 0.45$) is attributable to an increased exciton binding energy in indirect material.
- ²⁹R. E. Anderson, D. J. Wolford, and B. G. Streetman, *J. Appl. Phys.* **48**, 2453 (1977).
- ³⁰F. Bassani, G. Iadonisi, and B. Preziosi, *Rep. Prog. Phys.* **37**, 1099 (1974).
- ³¹M. A. Lampert, *Phys. Rev. Lett.* **1**, 450 (1958).
- ³²J. L. Merz, R. A. Faulkner, and P. J. Dean, *Phys. Rev.* **188**, 1228 (1969).
- ³³The possibility that N_Γ is emission from a molecule of two interacting N_x excitons appears to be inconsistent with the expected small interaction energy and the fact that N_Γ appears to follow the Γ_1 band edge.
- ³⁴The breadth of the spectra has frustrated attempts to observe absorption by a single N_Γ exciton. No attempt has been made to observe the various molecular states of the excitonic molecule.
- ³⁵It is conceivable that the N_x exciton bound to the nitrogen sufficiently alters the binding potential for an N_Γ exciton that a bound N_Γ state exist only as a molecule, and that hence N_Γ should not be observed in absorption.
- ³⁶J. W. Allen, *J. Phys. C* **1**, 1136 (1968); **4**, 1936 (1971).
- ³⁷J. R. Chelikowsky and M. L. Cohen, *Phys. Rev. B* **14**, 556 (1976).
- ³⁸M. L. Cohen and V. Heine, *Solid State Phys.* **24**, 37 (1970).
- ³⁹J. M. Luttinger and W. Kohn, *Phys. Rev.* **97**, 869 (1955); W. Kohn and J. M. Luttinger, *ibid.* **98**, 915 (1955).
- ⁴⁰The effective-mass approximation of Luttinger and Kohn is formally derived for smoothly varying potentials. It has also been applied to deep and localized traps with considerable success, the best known example being the Mott-Littleton theory of F centers in alkali halides [see, for instance, G. Iadonisi and B. Preziosi, *Nuovo Cimento B* **48**, 92 (1967), and references therein].
- ⁴¹The spherical square well that yields a good fit to the data in the composition range $0.28 \leq x \leq 0.45$ is
- $$V(\vec{r}) = \begin{cases} -V_0, & |\vec{r}| \leq a, \\ 0, & \text{otherwise,} \end{cases}$$
- where the empirical parameters V_0 and a are given by
- $$V_0 = (0.66 - 1.08x) \text{ eV,}$$
- and $a = (7.45 + 45.33x) \text{ \AA.}$
- ⁴²R. J. Stirn, in *Semiconductors and Semimetals*, edited by R. K. Willardson and A. C. Beer (Academic, New York, 1972), Vol. 8, p. 49.
- ⁴³B. W. Hakki, *J. Appl. Phys.* **42**, 4981 (1971).
- ⁴⁴J. Callaway, *J. Math. Phys.* **5**, 783 (1964).
- ⁴⁵The deformation potential associated with the nitrogen impurity is chosen to have tetrahedral (T_d) symmetry for purely mathematical convenience. Both GaAs and GaP are elastically anisotropic, with $K \equiv 2C_{44}/(C_{11} - C_{12})$ being 1.82 and 1.79, respectively [R. M. Martin, *Phys. Rev. B* **1**, 4005 (1970)]; these values are to be contrasted with the anisotropic ($K=2$) and isotropic ($K=1$) limits, respectively. It can be shown [J. R. Hardy and R. Bullough, *Philos. Mag.* **15**, 237 (1967); J. D. Eshelby, *Solid State Phys.* **3**, 79 (1956)] that such anisotropic crystals produce dilational deformation potentials varying asymptotically as $\text{div } \vec{u} \sim (2/5r^3) - 2r^{-1}(x^2y^2 + y^2z^2 + x^2z^2)$.
- ⁴⁶M. Tinkham, *Group Theory and Quantum Mechanics* (McGraw-Hill, New York, 1964).
- ⁴⁷R. A. Faulkner, *Phys. Rev.* **175**, 991 (1968).
- ⁴⁸G. F. Koster, J. O. Dimmock, R. G. Wheeler, and H. Statz, *Properties of the Thirty-two Point Groups* (MIT, Cambridge, Mass., 1963).
- ⁴⁹M. Jaros and S. F. Ross, *J. Phys. C* **6**, 1753 (1973); M. Jaros and S. Brand, *Phys. Rev. B* **10**, 4494 (1976).

⁵⁰L. Vegard, *Z. Phys.* **5**, 17 (1921).

⁵¹R. J. Nelson, N. Holonyak, Jr., J. J. Coleman, D. Lazarus, D. L. Keune, W. O. Groves, and M. G. Craford, *Phys. Rev. B* **14**, 3511 (1976).

⁵²R. J. Nelson, N. Holonyak, Jr., J. J. Coleman, D. Lazarus, D. L. Keune, A. H. Herzog, W. O. Groves, and G. G. Kleiman, *Appl. Phys. Lett.* **29**, 615 (1976).

⁵³J. D. Cuthbert and D. G. Thomas, *Phys. Rev.* **154**, 763 (1967).

⁵⁴R. J. Nelson and N. Holonyak, Jr., *Solid State Commun.* **20**, 549 (1976).

⁵⁵W. Y. Hsu, J. D. Dow, D. J. Wolford, B. G. Streetman, Y. Makita, and S. Gonda (unpublished).

⁵⁶Y. Sugiura, *Z. Phys.* **45**, 484 (1927).

⁵⁷C. C. J. Roothaan, *J. Chem. Phys.* **19**, 1445 (1951).

⁵⁸P. J. Wiesner, R. A. Street, and H. D. Wolf, *Phys. Rev. Lett.* **35**, 1366 (1975).

⁵⁹In the four cases of Table VI where the representation contains $2A_1$ irreducible representations, it is always possible to take

$$|A_1 1s\rangle = n_s^{-1/2} \sum_{\sigma=1}^{n_s} |W(\vec{R}_{s,\sigma})\rangle$$

and

$$|A_1 2s\rangle = n_s^{-1/2} \sum_{\sigma=1}^{n_s} \pi_{\sigma} |W(\vec{R}_{s,\sigma})\rangle,$$

where $\pi_{\sigma} = 1$ if $\vec{R}_{s,\sigma}$ is obtainable by a group operation on $\vec{R}_{s,1}$ and $\pi_{\sigma} = -1$ if it is not. The two states are orthogonal and matrix elements of GV with $|A_1 1s\rangle$ and $|A_1 2s\rangle$ are zero. Note that it is easiest to take $\vec{R}_{s,1} = \frac{1}{2} a_L(\mu, \nu, \lambda)$, where $\mu \geq \nu \geq \lambda \geq 0$ are integers with an even sum.

⁶⁰See, for example, G. Gilat, in *Methods in Computational Physics*, edited by G. Gilat (Academic, New York, 1976), Vol. 15, p. 317.

⁶¹D. J. Chadi and M. L. Cohen, *Phys. Rev. B* **8**, 5747 (1973); and *Solid State Commun.* **13**, 1007 (1973).

⁶²M. L. Cohen and T. K. Bergstresser, *Phys. Rev.* **141**, 789 (1966).

⁶³The composition dependences of the band edges are taken from several sources, including recent data. The choice of parameters is discussed in Ref. 1.